Received: 24 May 2024 | Revised: 11 September 2024 | Accepted: 12 September 2024

DOI: 10.1002/pamm.202400143

RESEARCH ARTICLE

Experimental characterization of acoustic damping materials

Paul Marter[1] | **Lars Radtke**[2] | **Sascha Eisenträger**[1] | **Alexander Düster**[2] | **Daniel Juhre**[1]

[1]Institute of Mechanics, Otto von Guericke University Magdeburg, Magdeburg, Germany

[2]Numerical Structural Analysis with Application in Ship Technology, Institute for Ship Structural Design and Analysis, Hamburg University of Technology, Hamburg, Germany

Correspondence
Paul Marter, Institute of Mechanics, Otto von Guericke University Magdeburg, Magdeburg, Germany.
Email: paul.marter@ovgu.de

Funding information
DFG, Grant/Award Number: 503865803

Abstract

Due to their ease of use and low cost, passive damping methods are a preferred mean for the reduction of noise in many engineering applications. This applies in particular to foam materials, which exhibit good acoustic and mechanical damping properties. The selection of suitable materials is usually carried out experimentally and can be very labor-intensive and time-consuming. For this reason, it is helpful to develop qualified numerical methodsthat can be used for material design and selection. Hence, foam materials must be characterized experimentally in order to enable a later comparison with vibroacoustic simulations. This contribution, therefore, aims at providing suitable parameters for the use in numerical analyses and their validation. Firstly, the microstructure of a foam specimen is captured by means of a CT scan. In addition to providing the geometry for the multi-physics simulations, this measurement is also used to determine characteristic foam features, for example, strut thickness and pore size distribution. In the second step, the frequency-dependent stiffness and damping properties of the material are determined by a special experimental setup utilizing an electrodynamic shaker. Here, the dynamic system is approximated as a single-mass oscillator, which is sufficiently accurate for low frequencies. These properties will later be used in the numerical model to evaluate different parameter identification approaches. In the third and last step of the experimental campaign, measurements with an impedance tube are conducted to obtain the coefficient of absorption. This material parameter is particularly suitable for comparing experiments and simulations. Finally, the correlation between the experimental results is examined to provide a deeper understanding of the foam materials.

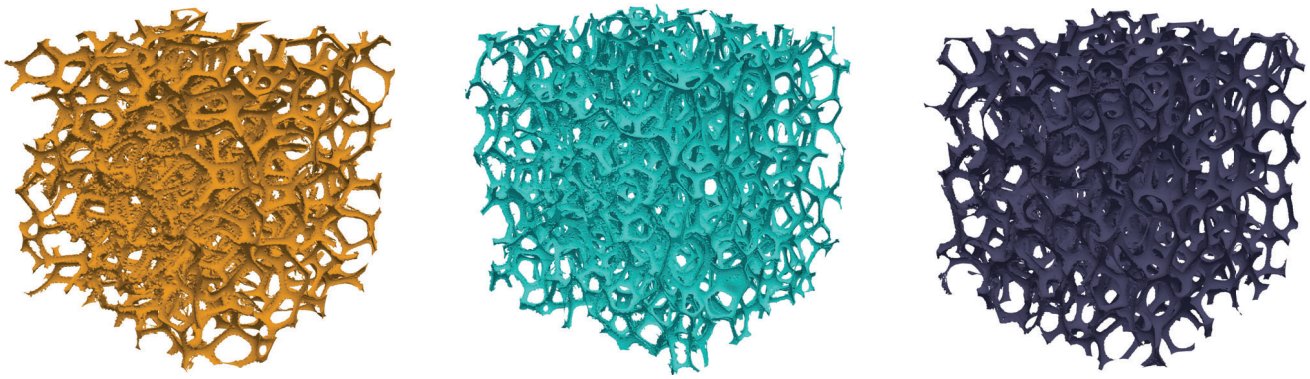

FIGURE 1 Visualization of the micro-structure for the three foam materials under investigation: foam_A, foam_B, foam_C (from left to right).

1 | MOTIVATION

Acoustic design plays an important role in a wide range of applications across various industries, spanning from automotive engineering and aerospace to architectural construction and consumer electronics. In each of these areas of application, the effective management of sound is of great relevance, whether it involves reducing noise pollution, enhancing speech intelligibility, or improving overall auditory comfort. During the design process, it is often required to reduce undesired vibrations in a structure, which in general, are caused by an acoustic source emitting a sound power. This power is transported through the air as sound waves until it encounters a surface with varying acoustic impedance. The energy is partly reflected, transmitted, or absorbed there. In addition, a portion can also be introduced into the structure and propagate as structure-borne sound. This behavior can be expressed by the equation

$$P_{\mathrm{total}} = P_{\mathrm{r}} + P_{\mathrm{t}} + P_{\mathrm{s}} + P_{\mathrm{a}} \tag{1}$$

with the total sound power P_{total}, the reflected part P_{r}, the transmitted part P_{t}, the power converted into structure-borne sound P_{s}, and the absorbed (dissipated) sound power P_{a}. In order to reduce unwanted vibrations, passive damping materials such as polyurethane (PUR) foams are applied primarily to increase the amount of the absorbed sound power. Foams have received significant attention in various industries due to their lightweight nature, thermal insulation properties, and acoustic damping capabilities. Furthermore, these materials offer cost-effectiveness and simplicity in their application to any given structure [2]. However, the selection of suitable passive damping materials can be cumbersome, since the material has to adhere to various requirements in order to reduce both air-borne and structure-borne noise in individual applications. Therefore, understanding the properties of such foams is crucial for optimizing their performance in practical applications.

Numerical simulation models can be used to gain deeper insights into the material behavior and a better understanding of the internal damping processes. For this purpose the finite cell method (FCM), first proposed in refs. [3, 4], has been extended for vibroacoustical problems [5]. This allows us to fully resolve the microstructure of the foam material by an automated meshing procedure and to investigate the fluid-structure interaction within the material. We plan to certify the numerical models proposed in ref. [1] as a tool for improved material selection in particular applications. Therefore, the presented research is divided into two parts: (i) an experimental campaign is conducted to fully characterize the properties of the foam materials (done in this paper) and (ii) numerical simulations are run using the identified material properties as a basis (done in ref. [1]).

Since numerical models lack utility without proper validation, acquiring information on the material properties is necessary. These are obtained from the experiments conducted within the scope of this study. In the contribution at hand, we determine the microstructure [6], the static and dynamic structural properties [7, 8] as well as the acoustic properties [9, 10] of three different PUR foams varying in volume weight between 24 kg/m^3 and 39 kg/m^3. The microstructure of these foams with the corresponding volume weight is shown in Figure 1. In summary, this study endeavors to advance the

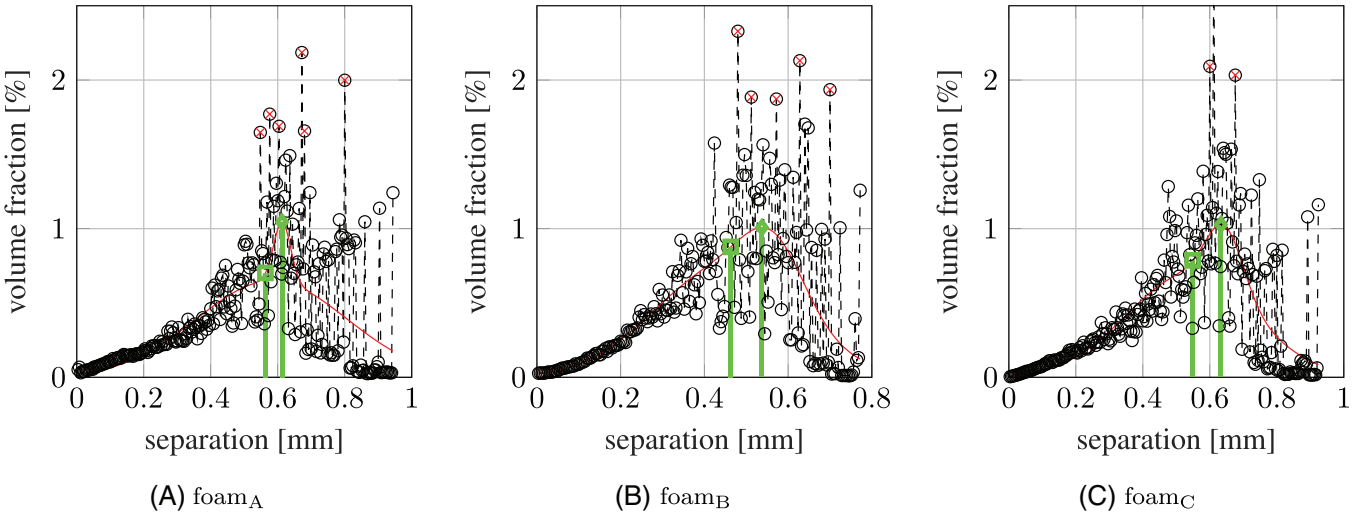

FIGURE 2 Pore size distribution of foam$_A$, foam$_B$ and foam$_C$ (from left to right) given as the volume fraction over the midpoint of the particular size range. Shown is the distribution of the binarized data (dotted line), the Gaussian fit (red line) as well as the maximum (diamond) and the center of gravity (square) of the Gaussian fit (green line). Outliers were identified and disregarded to improve the quality of the fit.

understanding of acoustic PUR foam materials through rigorous experimental characterization, laying the groundwork for the development of effective numerical models for predicting their acoustic behavior [1].

2 | EXPERIMENTS

To determine the material properties of the presented foams, we used different experimental setups explained in detail in this section. While very small specimen dimensions were necessary for the microscopic characterization, the same specimens could be used for all macroscopic characterization experiments with a dimension of ∅30 mm × 30 mm for foam$_A$ and foam$_B$ and ∅30 mm × 15 mm for foam$_C$. Different dimensions result from the availability of the mat material provided by the manufacturer, which were selected on the recommendation of the manufacturer to ensure variation in the microstructure. The specimens for the macroscopic tests were cut by hand with a scroll saw from the mat material.

2.1 | Determination of the microstructure using X-Ray CT

In a first experiment, we captured the microstructure of the foams by an X-ray computed tomography (CT), revealing the spatial distribution of cell and strut sizes, shapes, and connectivity, shedding light on foam density, porosity, and overall mechanical properties. As a result, we get a sequence of 1800 images each with 1800 × 1800 voxels. Leading to a captured specimen size of $3.6 \times 3.6 \times 3.6\,\mathrm{mm}^3$ based on a resolution of 2 µm per voxel. For the evaluation of the pore and strut size distributions as well as to serve as a basis for the numerical model, the grayscale images from the CT scans need to be binarized. For this step, we used the open-source software package *3D Slicer* [11]. Depending on some segmentation settings, it is possible to discretize the microstructure as an STL file. The corresponding foam structures are visualized in Figure 1. The STL data is used as input for the simulation pipeline to perform an inside-outside test.

Additionally, the pore and strut size distribution is evaluated based on the binarized data. Figure 2 shows the pore size distribution for the three foam materials. For the evaluation, the determined characteristic lengths are divided into evenly distributed ranges, and the volume fraction of each range is plotted over the midpoint of the particular range. After identifying and removing outliers from the data set, a two-term Gaussian function with seven parameters

$$f(x) = a\,\mathrm{e}^{-(x-b)/c} + d\,\mathrm{e}^{-(x-f)/g} + h$$

TABLE 1 Identified pore and strut sizes for the investigated materials.

	Foam_A		Foam_B		Foam_C	
	Pore	**Strut**	**Pore**	**Strut**	**Pore**	**Strut**
Center of gravity (mm)	0.536	0.018	0.463	0.037	0.549	0.040
Maximum (mm)	0.613	0.019	0.538	0.030	0.633	0.033

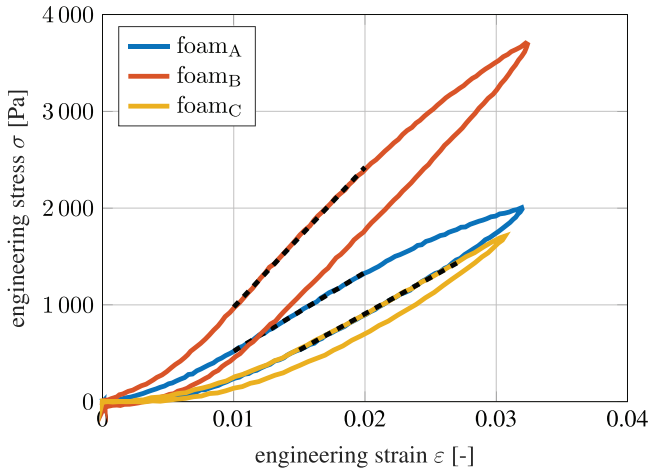

FIGURE 3 Results from the static compression tests with a linear loading and unloading process shown as the stress-strain curves for all three foams. Only small amplitudes were considered and the identified linear section is highlighted as a dashed line for evaluating an approximated Young's modulus.

can be fitted to the measurement data. This is justified by considering not only the pore sizes, but also the windows between the open cells of the foam and the struts and their junctions, respectively. For each Gaussian function, the maximum and the center of gravity can be calculated so that it is possible to compare the distribution of the pore and strut sizes between the materials.

Table 1 summarizes the determined distributions of all three materials. First of all, it can be seen that the strut size correlates with the volume weight of the material. Moreover, the investigated materials provide good variety in the microstructure with different combinations of pore and strut sizes for each foam. After introducing the other experimental results, a relation between the microstructure and the mechanical and acoustical properties is drawn.

2.2 | Determination of the structural static properties

Having identified the microstructure of the materials, we determined the macroscopic material properties starting with static compression tests. We conducted the compression tests employing a linear loading and unloading process up to a defined displacement value in the direction of the foam rise (thickness direction) measuring the resulting force during the deformation process. Quasi-static conditions were ensured using only a small strain rate of 0.01 mm/s.

Considering only a small displacement amplitude, it is justified to calculate engineering stresses and strains from the measured forces F and displacements u with $\sigma = F/A_0$ and $\varepsilon = u/L_0$, resulting in the stress-strain curves shown in Figure 3. Here, A_0 and L_0 are the cross-section area and the initial length of the ideal specimen shape. The progressive stiffness for the initial displacements is assumed to be a setting behavior due to slight deviations from the ideal shape of the specimens causing an initial inhomogeneous contact situation.

Despite the small amplitudes, a hysteresis behavior is still occurring for all three foams. Since the strain rate was kept very low, it can be assumed that the viscoelastic influences from the polymeric nature of the material are relatively small. It is therefore likely that the cause of the hysteresis lies in the foam's microstructure, for example, in the form of contact friction between individual struts or joints or static hysteresis, known from filled elastomers. A fully resolved simulation of the foam microstructure will help to get further insights into the internal processes. In the stress-strain curves of each foam, a segment displaying a linear behavior can be identified, facilitating the estimation of Young's modulus through

TABLE 2 Identified Young's moduli based on the linear region in the stress-strains curve for the three foams.

	Foam_A	Foam_B	Foam_C
Young's modulus (Pa)	$8.56 \cdot 10^4$	$14.20 \cdot 10^4$	$5.92 \cdot 10^4$

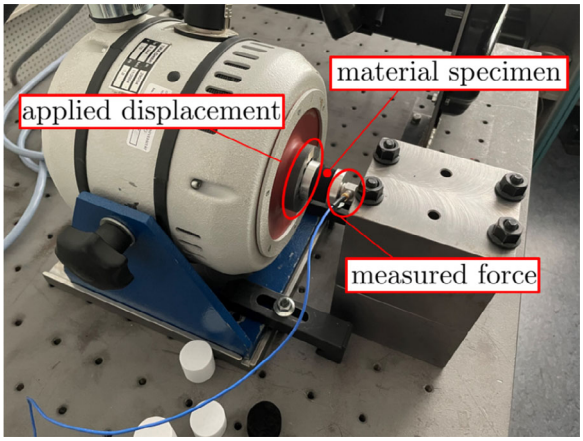

FIGURE 4 Test setup for the harmonic analysis utilizing an electrodynamic shaker.

linear regression analysis with $E = \Delta\sigma/\Delta\varepsilon$. Table 2 gives an overview of the identified Young's moduli. For each value, the average of five different specimens was calculated. Only for foam_A and foam_B, the stiffness correlates with the strut size and in this way also with the volume weight. This is because of a foaming process with similar polyol components for both materials. In contrast, different polyol components were used for foam_C resulting in a much smaller stiffness despite the higher volume weight. However, the exact composition of the materials is not known to the authors. This behavior highlights the importance of identifying not only the macroscopic stiffness properties but also the structural properties of the solid-state material in the foam.

2.3 | Determination of the structural dynamic properties

PUR belongs to the material class of polymers, which are known for their viscoelastic material behavior. For this reason, it is important to determine also the dynamic properties of the investigated foams. This was done by a harmonic analysis utilizing an electrodynamic shaker [7], which is shown in Figure 4. For the evaluation of the dynamic properties, a harmonic displacement with a constant frequency f

$$u(t) = \hat{u} \cdot \sin(2\pi f t) \tag{2}$$

is applied to the material specimen and measured by a laser Doppler vibrometer. Here, the displacement amplitude $\hat{u}$ was chosen very small with 25 μm to reflect real application examples. Additionally, the resulting harmonic force is captured by a sensor placed on the opposite side of the specimen

$$F(t) = \hat{F} \cdot \sin(2\pi f t + \delta). \tag{3}$$

To ensure a linear material behavior, the specimens for all foams were preloaded so that the dynamic amplitude was applied in the previously identified linear region of each foam (see Figure 3). Due to the viscoelastic properties of the foams, a phase shift δ occurs between the input and the output signal. Figure 5 depicts a snapshot of the captured time signals for both the displacement and the force. The measurement data can be noisy for particular measurements. Thus, the amplitude is averaged in the evaluation period.

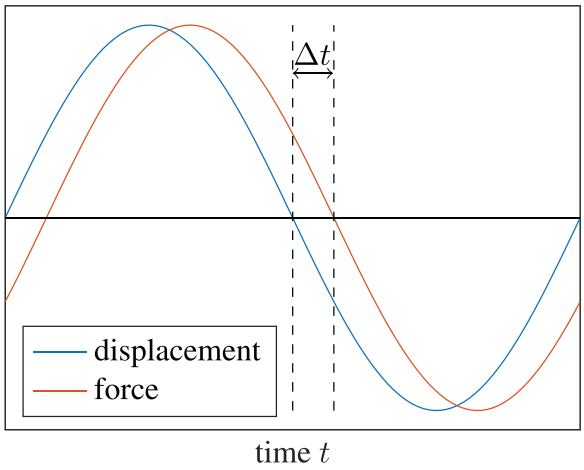

FIGURE 5 Schematic illustration of the time curves for the measured displacement and force signals with a time lag Δt.

The dynamic material properties are expressed in terms of the storage modulus

$$E' = \frac{\hat{\sigma}}{\hat{\varepsilon}}\cos(\delta) \tag{4}$$

and the loss modulus

$$E'' = \frac{\hat{\sigma}}{\hat{\varepsilon}}\sin(\delta), \tag{5}$$

which can be used to define the complex modulus

$$E^* = E' + iE'' \tag{6}$$

and a measure of the material damping

$$\tan\delta = \frac{E''}{E'} \tag{7}$$

for the materials. Under the condition of small strains, that is, in the linear region of the material, the stress and strain amplitudes can be again calculated by $\hat{\sigma} = \hat{F}/A_0$ and $\hat{\varepsilon} = \hat{u}/L_0$, respectively. The phase shift δ is determined from the time signals of the measurement data considering the time difference Δt for a given frequency f

$$\delta = \omega\Delta t \qquad \text{with} \qquad \omega = 2\pi f. \tag{8}$$

The storage and loss moduli calculated for a range from 10 to 500 Hz are depicted in Figure 6. An increasing storage modulus over the frequency can be observed which is a common trend for polymers and other viscoelastic materials lacking a crystalline structure [12, 13]. When comparing the storage moduli of the three foams, it becomes evident that their dynamic stiffness properties are governed by the same microstructural properties that are also decisive for the statically identified Young's moduli. This alignment is discernible from the consistent order of Young's and storage modulus across the foams. This is not true for the loss modulus, where $\mathrm{foam_C}$ can achieve a higher damping effect as $\mathrm{foam_A}$ and $\mathrm{foam_B}$ despite the smaller dynamic stiffness. This underlines the influence of the particular material composition on the structural properties of the foams which differs between $\mathrm{foam_C}$ and the other two.

2.4 | Determination of the acoustical properties

As a last macroscopic characterization experiment, we determined the acoustical properties employing an impedance tube according to EN ISO 10534-2 [14]. The schematic test setup is illustrated in Figure 7. The measurement principle is based on

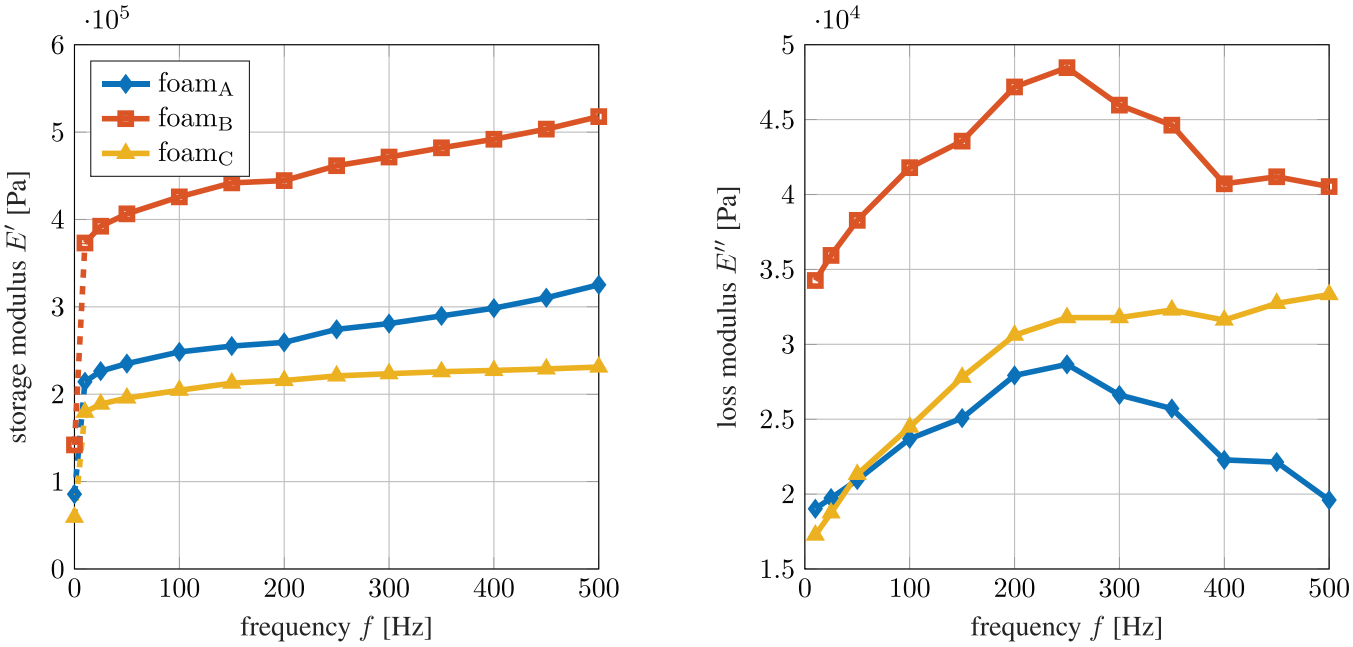

FIGURE 6 Storage and loss moduli E' and E'' for the three foams.

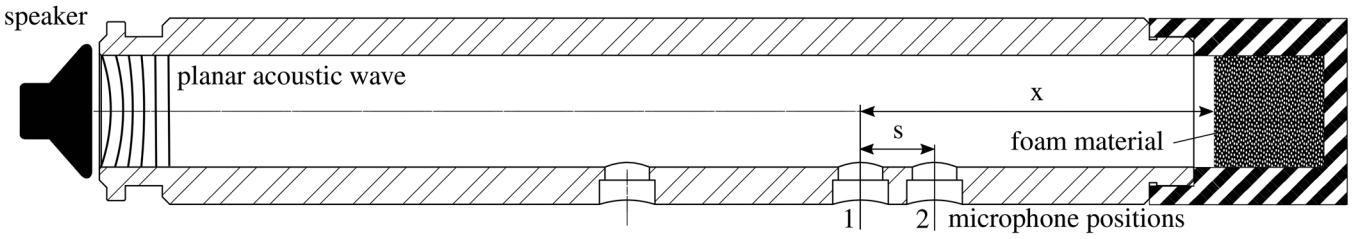

FIGURE 7 Schematic illustration of an impedance tube for the determination of the reflection and the absorption coefficient.

planar acoustic waves in the tube radiated by a speaker along the tube axis. This condition is fulfilled as long as a particular ratio between the diameter and the wavelength of interest is guaranteed. For this reason, different tube diameters have to be used depending on the investigated frequency range. We used a diameter of 100 mm for the frequency range from 100 to 1600 Hz and a diameter of 30 mm for the range from 1600 to 6200 Hz. The specimen is placed on the opposite side of the speaker in front of a sound-reflecting end cap where the incoming sound wave is reflected.

To determine the acoustic properties, the sound pressure is measured at two different locations which can be done in two different ways. For a harmonic signal input, the microphone positions need to be varied to find the maximum and minimum pressure values of the emerging standing wave in the tube. With fixed microphone positions having the defined distance s, a pseudo-random signal is used as input to evaluate the coefficient of reflection in the defined frequency range of the input signal. Based on the complex sound pressure values p_{1I}/p_{2I} and p_{1R}/p_{2R}, the transfer functions for the incoming wave

$$H_I = \frac{p_{2I}}{p_{1I}} = e^{-jk_0 s} \tag{9}$$

and for the reflected wave

$$H_R = \frac{p_{2R}}{p_{1R}} = e^{jk_0 s} \tag{10}$$

can be calculated with the complex wave number k_0. Taking into account also the transfer function H_{12} between both, microphone positions and the distance between the first microphone position and the surface of the foam specimen x,

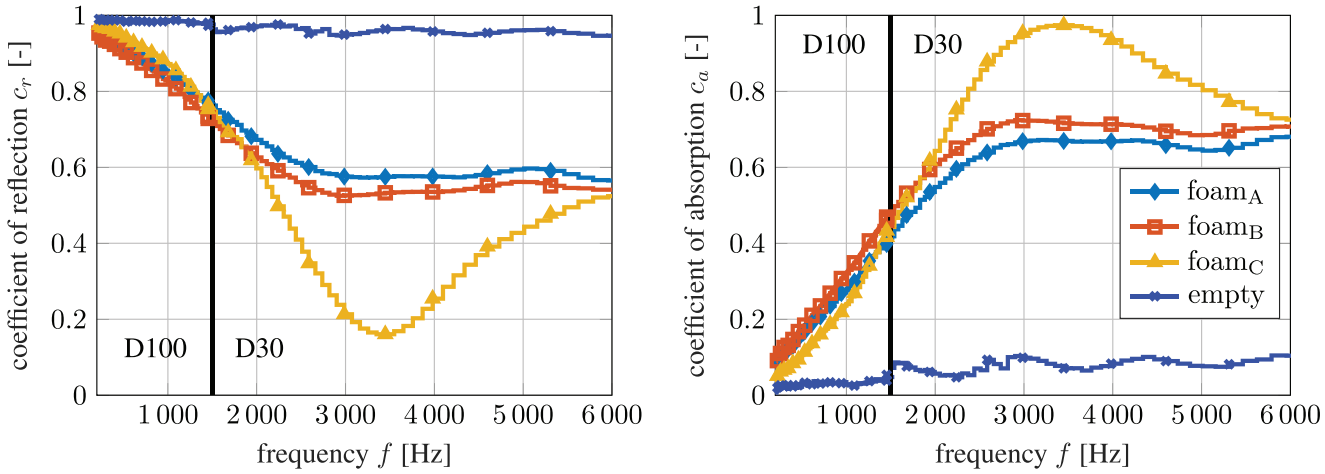

(a) Coefficient of reflection.

(b) Coefficient of absorption.

FIGURE 8 Determined acoustical properties of the foams.

the coefficient of reflection

$$c_r = \frac{H_{12} - H_I}{H_R - H_{12}} e^{2jk_0x} \tag{11}$$

can be determined. Subsequently, the coefficient of absorption

$$c_a = 1 - |c_r|^2 \tag{12}$$

can be calculated.

Figure 8 shows the determined coefficient of reflection (Figure 8(a)) and the coefficient of absorption (Figure 8(b)) for the three foam materials. In the first step, we identified the measurement uncertainty by conducting an empty measurement. Since the experimental setup is not an ideally closed system, dissipation can occur during the measurement, resulting in a reflection coefficient smaller than one for an empty tube. However, the losses are relatively small so that the reflection coefficients determined for the foam materials are clearly distinguishable from the empty measurement. All materials show a linear region for lower frequencies reaching a plateau for higher frequencies. This behavior is caused by different dissipation processes. While thermal dissipation has a major influence on the low-frequency regime, viscous dissipation dominates in the higher frequency range [10]. Despite their different structural properties, foam$_A$ and foam$_B$ seem to have similar acoustic properties. Foam$_C$ with the highest volume weight and the lowest stiffness shows the best acoustic properties in terms of a high absorption coefficient.

3 | SUMMARY AND OUTLOOK

In this work, we characterized three different PUR foams on the microscopic and the macroscopic scale identifying the structural and acoustical properties. The determined material data is summarized in Table 3. Taking a closer look at foam$_A$ and foam$_B$, it can be seen that the average strut size determines the volume weight as well as the static and dynamic stiffness properties. Additionally, a larger pore size does not guarantee that a higher acoustic absorption can be achieved. Since different additives were used in the foaming process for foam$_C$, the results can not be directly compared to the other two foams which require a detailed material analysis. Foam$_C$ shows the best acoustical and structural damping properties having the highest volume weight and the largest pore size. But despite the large strut size, foam$_C$ has the lowest stiffness properties. Considering also the results from foam$_A$ and foam$_B$, the results indicate a correlation between material damping and acoustic absorption which will be investigated in more detail in further work.

TABLE 3 Summary of the identified material properties for the PUR foams.

Property	Unit	$Foam_A$	$Foam_B$	$Foam_C$
Volume weight	(kg/m^3)	23.88	29.81	39.31
Average pore diameter	(mm)	0.536	0.463	0.549
Average strut diameter	(mm)	0.018	0.037	0.040
Young's modulus	(Pa)	$8.56 \cdot 10^4$	$14.20 \cdot 10^4$	$5.92 \cdot 10^4$
Dynamic stiffness	–	Medium	Highest	Lowest
Structural damping	–	Lowest	Medium	Highest
Acoustic absorption	–	Lowest	Medium	Highest

Abbreviation: PUR, polyurethane.

In future work, the identified material characteristics will be used to build a suitable numerical model. This will allow further insights into the damping processes based on the material characteristics and will finally help to accelerate the design process of passive damping materials featuring a porous microstructure.

ACKNOWLEDGMENTS

The authors gratefully acknowledge the support of the DFG (Deutsche Forschungsgemeinschaft), Germany under DU 405/20-1 and DU 1904/5-1 (grant number 503865803).

Open access funding enabled and organized by Projekt DEAL.

ORCID

Paul Marter https://orcid.org/0000-0001-5937-6158
Lars Radtke https://orcid.org/0000-0001-7015-8928
Daniel Juhre https://orcid.org/0000-0001-8997-3818

REFERENCES

1. Radtke, L., Marter, P., Eisenträger, S., Juhre, D., & Düster, A. (2024). An automatic simulation pipeline for coupled simulations of acoustic damping materials. *Proceedings in Applied Mathematics and Mechanics*, *24*, e202400093.
2. Duvigneau, F., Luft, T., Hots, J., Verhey, J. L., Rottengruber, H., & Gabbert, U. (2016). Thermo-acoustic performance of full engine encapsulations – A numerical, experimental and psychoacoustic study. *Applied Acoustics*, *102*, 79–87.
3. Parvizian, J., Düster, & Rank, E. (2007). Finite cell method: h- and p-extension for embedded domain problems in solid mechanics. *Computational Mechanics*, *41*(1), 121–133.
4. Düster, A., Parvizian, J., Yang, Z., & Rank, E. (2008). The finite cell method for three-dimensional problems of solid mechanics. *Computer Methods in Applied Mechanics and Engineering*, *197*(45–48), 3768–3782.
5. Radtke, L., Marter, P., Duvigneau, F., Eisenträger, S., Juhre, D., & Düster, A. (2024). Vibroacoustic simulations of acoustic damping materials using a fictitious domain approach. *Journal of Sound and Vibration*, *568*(January), 118058.
6. Patterson, B. M., Henderson, K., Gilbertson, R. D., Tornga, S., Cordes, N. L., Chavez, M. E., & Smith, Z. (2014). Morphological and performance measures of polyurethane foams using x-ray CT and mechanical testing. *Microscopy and Microanalysis: The Official Journal of Microscopy Society of America, Microbeam Analysis Society, Microscopical Society of Canada*, *20*(4), 1284–1293.
7. Spannan, L., Duvigneau, F., Gavila Lloret, M., Daniel, C., Juhre, D., & Woschke, E. (2020). A study on harmonic excitation based experimental characterization of damping materials for acoustic simulations. *Technische Mechanik - European Journal of Engineering Mechanics*, *40*(2), 134–148.
8. Petrů, M., & Novák, O. (2017). Measurement and numerical modeling of mechanical properties of polyurethane foams. In F. Yılmaz (Ed.), *Aspects of Polyurethanes*. InTech. https://doi.org/10.5772/intechopen.69700
9. Pompoli, F., Bonfiglio, P., Horoshenkov, K. V., Khan, A., Jaouen, L., Bécot, F. X., Sgard, F., Asdrubali, F., D'Alessandro, F., Hübelt, J., Atalla, N., Amédin, C. K., Lauriks, W., & Boeckx, L. (2017). How reproducible is the acoustical characterization of porous media?. *The Journal of the Acoustical Society of America*, *141*(2), 945–955.
10. Atalla, Y., & Panneton, R. (2005). Inverse acoustical characterization of open cell porous media using impedance tube measurements. *Canadian Acoustics*, *33*(1), 11–24.
11. Jolesz, F. A. (2014). *Intraoperative Imaging and Image-Guided Therapy* (1st ed.). Springer.
12. Ferry, J. D. (1980). *Viscoelastic properties of polymers* (3rd ed.) John Wiley & Sons.

13. Sfaoui, A. (1995). On the viscoelasticity of the polyurethane foam. *The Journal of the Acoustical Society of America*, *97*(2), 1046–1052.
14. EN ISO 10534-2:2001. https://www.dinmedia.de/de/norm/din-en-iso-10534-2/40808828

How to cite this article: Marter, P., Radtke, L., Eisenträger, S., Düster, A., & Juhre, D. (2024). Experimental characterization of acoustic damping materials. *Proceedings in Applied Mathematics and Mechanics*, *24*, e202400143. https://doi.org/10.1002/pamm.202400143